JACS
JOURNAL OF THE AMERICAN CHEMICAL SOCIETY

Article

pubs.acs.org/JACS

Photoinduced Electron Transfer within Supramolecular Donor–Acceptor Peptide Nanostructures under Aqueous Conditions

Allix M. Sanders,[†,⊥] Timothy J. Magnanelli,[†] Arthur E. Bragg,[†] and John D. Tovar*[,†,‡,§]

[†]Department of Chemistry, Krieger School of Arts and Sciences, Johns Hopkins University, 3400 North Charles Street, Baltimore, Maryland 21218, United States

[‡]Department of Materials Science and Engineering, Whiting School of Engineering, Johns Hopkins University, 3400 North Charles Street, Baltimore, Maryland 21218, United States

[§]Institute of NanoBioTechnology, Johns Hopkins University, 3400 North Charles Street, Baltimore, Maryland 21218, United States

Supporting Information

ABSTRACT: We report the synthesis, self-assembly, and electron transfer capabilities of peptide-based electron donor–acceptor molecules and supramolecular nanostructures. These modified peptides contain π-conjugated oligothiophene electron donor cores that are peripherally substituted with naphthalene diimide electron acceptors installed via imidation of site-specific lysine residues. These molecules self-assemble into one-dimensional nanostructures in aqueous media, as shown through steady-state absorption, photoluminescence, and circular dichroism spectra, as well as transmission electron microscopy. Excitation of the oligothiophene donor moieties results in electron transfer to the acceptor units, ultimately creating polar, charge-separated states that persist for over a nanosecond as observed with transient absorption spectroscopy. This study demonstrates how transient electric fields can be engineered into aqueous nanomaterials of biomedical relevance through external, temporally controlled photonic inputs.

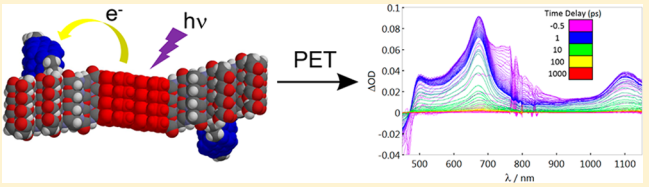

INTRODUCTION

π-Conjugated systems have been a mainstay of cutting-edge flexible electronics applications over the past decade, but more recently, attention has turned to their prospects in biological environments. Semiconducting, biocompatible materials based on organic electronic polymers and oligomers have been used to create a variety of bioelectronics devices that can be used for sensing/signaling[1−3] as well as for encouraging cell growth,[4−7] migration,[8] and differentiation.[9,10] However, the conductivity of the materials, i.e., the ability to create charge-carriers and generate electric fields, typically relies on the chemical doping or the use of external electronics. The next crucial step in the development of these materials for biomedical applications is to investigate the creation of such fields and carriers in the absence of chemical doping and external electronics. The use of transient local electric fields in a biological setting is well established (e.g., role of surface plasmons for biosensing), and the prospect for similar action in peptidic hydrogelators offers as yet uncharted opportunities for bioengineering.

Donor–acceptor systems capable of photoinduced charge transfer represent one possibility to generate electric fields. Nature uses photoinduced electron transfer to perform redox reactions, particularly in the process of photosynthesis, whereby initial excitations harvested by the photosynthetic pigments are transferred to a reaction center. Several synthetic mimics have been synthesized and studied to understand this process, typically involving the design of covalently bound donor–acceptor dyads, triads, and tetrads.[13−20] The covalent connection of complementary redox-active chromophores allows for charge transfer to not be limited by diffusion. Furthermore, the self-assembly of these donor–acceptor systems into supramolecular arrays encourages more rapid electron transfer kinetics.[21−25] These examples illustrate that supramolecular assemblies of covalently bound donor–acceptor chromophores, including those that rely on peptide assembly,[26−29] can be used to facilitate charge transfer and induce polar charge-separated states with low-energy photonic inputs. In fact, a π-conjugated donor–acceptor dyad was recently employed to report on the changes in local dielectric constant within a *de novo* designed α-helical protein during the charge separation process.[30]

Self-assembling peptide-based π-electron molecules (and their resulting nanomaterials) are promising targets to realize the photonic creation of charge-separated states.[11,12] Several groups have validated the ability of an oligopeptide assembly paradigm to be directly applicable to the supramolecular organization of π-electron structures.[31] These types of peptide–π-electron hybrids typically lead to optoelectronic nanomaterials whose photophysical properties are dictated by local geometries imposed on the π-electron moieties within the supramolecular assembly. More recently, tubular peptide-π-electron assemblies have validated the encouragement of excitonic energy migration within nanoscopic materials.[32] Indeed, we recently reported an energy donor–acceptor pair of peptidic π-electron molecules that co-assembled under

Received: November 16, 2015
Published: February 22, 2016

DOI: 10.1021/jacs.5b12001
J. Am. Chem. Soc. 2016, 138, 3362−3370

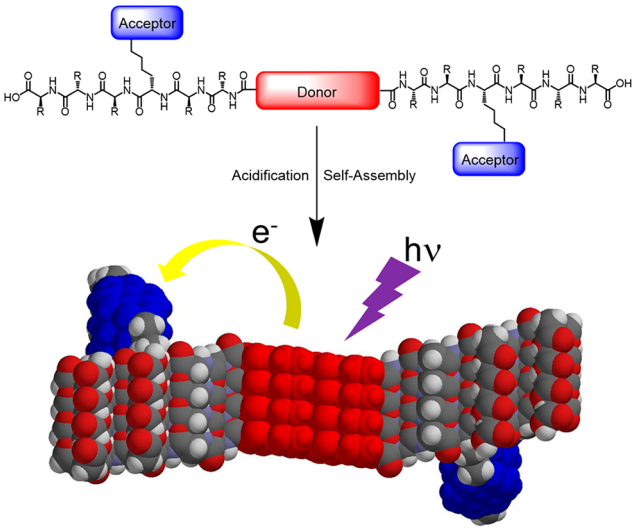

Figure 1. Illustration of self-assembly and electron transfer of a donor–acceptor π-peptide hybrid.

aqueous conditions and subsequently fostered energy migration to a low-energy "dopant",[33] in line with other recent studies on intercalated donor–acceptor peptide nanomaterials.[34,35]

In this Article, we describe a new direction in peptide-driven supramolecular polymerization of π-conjugated nanomaterials whereby electron-accepting groups are positioned pendant to a π-stacked electron donor core. These materials are a conceptual advance from the π-peptide hybrid systems that we previously studied,[36−38] in which solid-phase synthetic procedures were used to create novel peptides embedded with semiconducting π-conjugated subunits that could self-assemble in aqueous environments. To create π-stacked peptidic platforms capable of photoinduced electron transfer, acceptor units were incorporated onto amino acid side chains along peptide backbones that comprise a general self-assembling peptide–π-electron hybrid as illustrated in Figure 1. These molecules undergo a well-established pH assembly trigger, whereby changes in solution pH (in this case, a decrease in pH) allow for supramolecular self-assembly via the establishment of favorable intermolecular hydrogen bonding, ultimately creating noncovalent one-dimensional (1-D) nanostructures. Upon excitation of the internal donor moiety, energy migration and subsequent electron transfer to the peripheral acceptors can occur. In contrast to the seminal examples of donor–acceptor interactions waged in peptidic assemblies, where the nanomaterials are formed in organic solvents,[11,12] our molecular design allows for the manipulation of molecules and assemblies in completely aqueous environments.

RESULTS AND DISCUSSION

1. Dyad Design and Synthesis. *Design.* For the electron-donor unit, we chose quaterthiophene (OT4) because the synthesis of peptides embedded with this π-conjugated moiety has already been optimized.[37,38] Electron accepting naphthalene diimide (NDI) was selected for the acceptor, due to the option of facile incorporation via lysine side-chains. Venkataraman and co-workers have previously used this donor–acceptor pair in organic media and found it to be an ideal system for electron transfer due to the lack of spectral overlap between the emission wavelengths of OT4 and absorption wavelengths of NDI (to discourage nonpolar energy transfer) and beneficial LUMO level positioning (to encourage transfer of excited electrons).[39] We prepared a series of electron donor–acceptor pairs with varied separating peptide lengths alongside the analogous control molecules bearing the OT4 donor element only. These controls were used to dilute the donor–acceptor pair while at the same time being expected to foster exciton delocalization within the OT4 donor block prior to directing any excitations to the vicinity of the peptides with covalently attached NDI electron acceptors.

Synthesis. We used a general strategy to synthesize a series of key donor–acceptor dyads (**DA**) as well as the *N*-acylated control molecules (**C**) that vary in the spacing between the reactive lysine residues and the central OT4 core, as shown in Figure 2. The synthesis of the **DA** peptides (Scheme 1) began with the preparation of solid-supported oligopeptide sequences containing K(Mtt) residues (Mtt = 4-methyltrityl) placed specifically at different positions along the backbones, which were then *N*-acylated with 5-bromothiophene-2-carboxylic acid, as previously described.[20,21] Thus, three different "re-

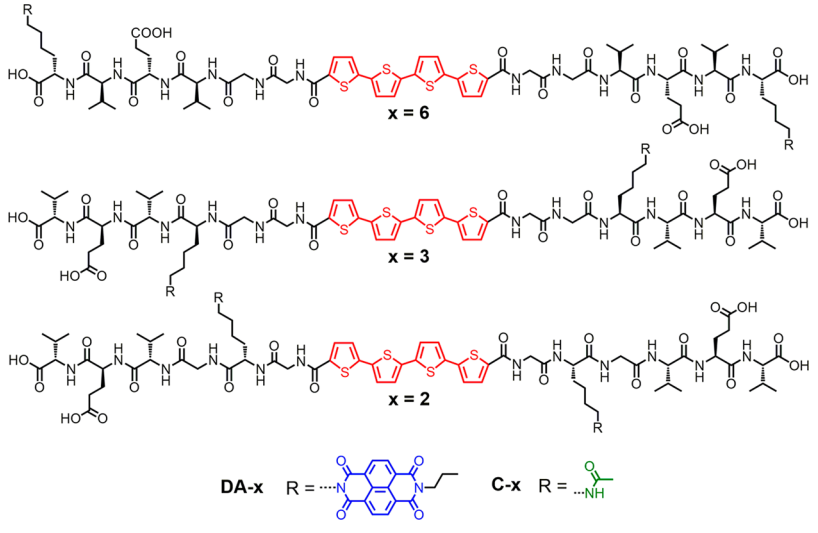

Figure 2. Structures of donor–acceptor (**DA-6**, **DA-3**, and **DA-2**) and acylated control (**C-6**, **C-3**, and **C-2**) peptides.

DOI: 10.1021/jacs.5b12001
J. Am. Chem. Soc. 2016, 138, 3362−3370

Scheme 1. Synthesis of DA-6 via Solid-Phase Stille Cross-Coupling and Imidation

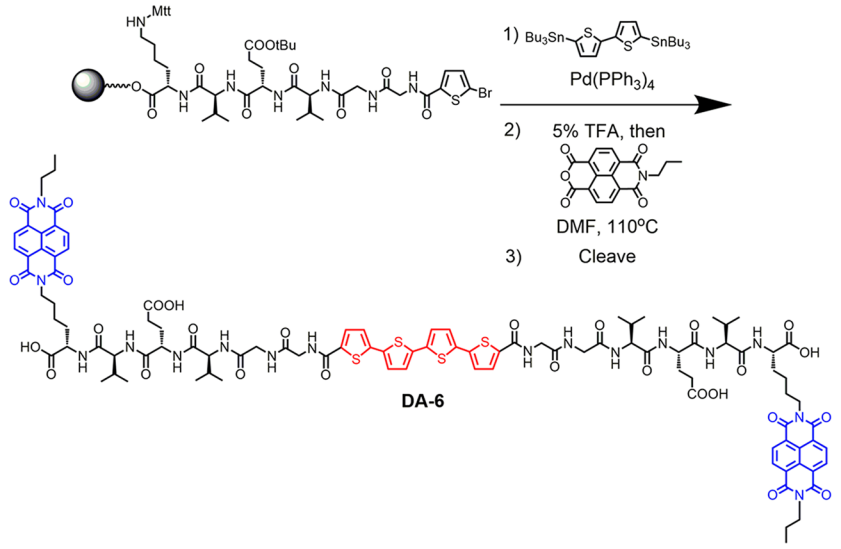

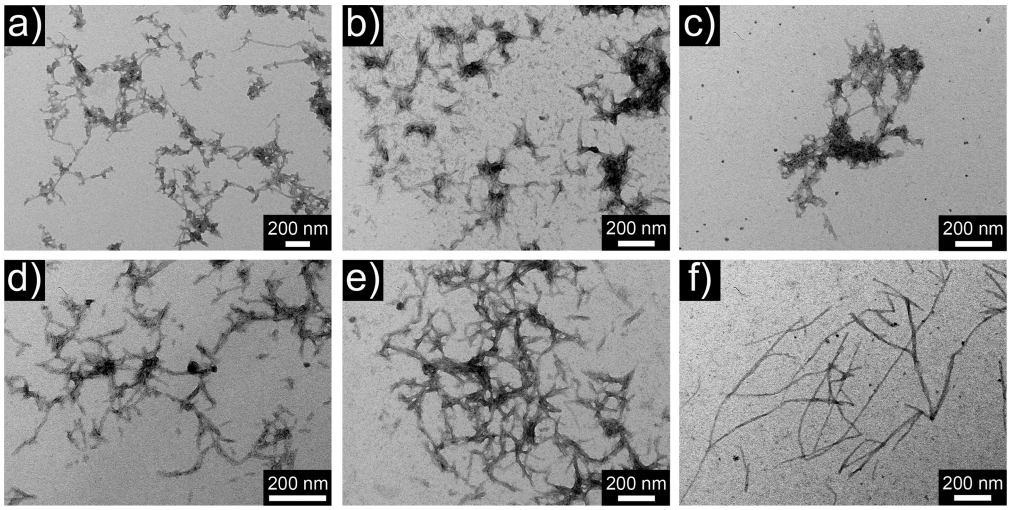

Figure 3. Transmission electron micrographs of (a) **DA-6**, (b) **DA-3**, (c) **DA-2**, (d) 25:75 **DA-6**:**C-6**, (e) 25:75 **DA-3**:**C-3**, and (f) 25:75 **DA-2**:**C-2**.

gioisomers" were prepared that vary by the position of the key K(Mtt) residue.

The resin-bound peptides were subjected to solid-phase Stille cross-coupling conditions in the presence of 5,5′-bis-(tributylstannyl)-2,2′-bithiophene, as previously described.[20] Next, the Mtt protecting groups were removed from the lysine residues by treatment with a 1% TFA cocktail, followed by imidation with *N*-propyl-1,4,5,8-naphthalenetetracarboxylic acid monoanhydride (to prepare the **DA** series)[40] or by *N*-acylation with acetic acid (to prepare the **C** series). The Mtt protecting group was chosen for the lysine residue because it can be removed in a weakly acidic environment, making it an orthogonal protecting group in Fmoc peptide synthesis. The resulting peptides were then cleaved from the resin (95% TFA) to give the final products. For example, the synthesis of **DA-6**, where the NDI acceptor is situated six amino acid residues away from the OT4 donor, is presented in Scheme 1.

To study the effect of donor−acceptor distance on the electron transfer capabilities of the peptides, **DA-3** and **DA-2** were synthesized using the same method, with donor−acceptor distances of three and two amino acids, respectively (Figure 2). The valine−glutamic acid−valine sequence was maintained in each peptide to preserve similar overall hydrophilicity/hydrophobicity of the peptide chains. Analogous control peptides **C-6**, **C-3**, and **C-2** were prepared, where the NDI-substituted lysine residues were replaced by *N*-acylated lysines (Figure 2). The controls were used to determine the contribution of the NDI acceptor unit on the electron transfer and assembly behavior of the peptides and also as a means to "dilute" the acceptor moieties within co-assembled mixtures of **DA-x** and **C-x**.

2. Structural Characterization of Dyad Assemblies. *Transmission Electron Microscopy.* The π-peptide hybrids are designed to maintain a relatively dissolved state in aqueous solution at high pH due to repulsion between negatively charged carboxylate groups. At low pH, the protonation of these groups reduces the Coulombic repulsion and triggers intermolecular self-assembly into 1-D nanostructures. TEM was employed to visualize these nanostructures and compare the assembly behavior of the neat donor−acceptor peptides (Figure 3a−c) and their co-assemblies with the relevant control peptides (in a 25:75 **DA**:**C** ratio, Figure 3d−f). In general, each peptide (co)assembly was comprised of 1-D nanostrutures displaying fairly uniform widths of 5−7 nm and significant

DOI: 10.1021/jacs.5b12001
J. Am. Chem. Soc. 2016, 138, 3362−3370

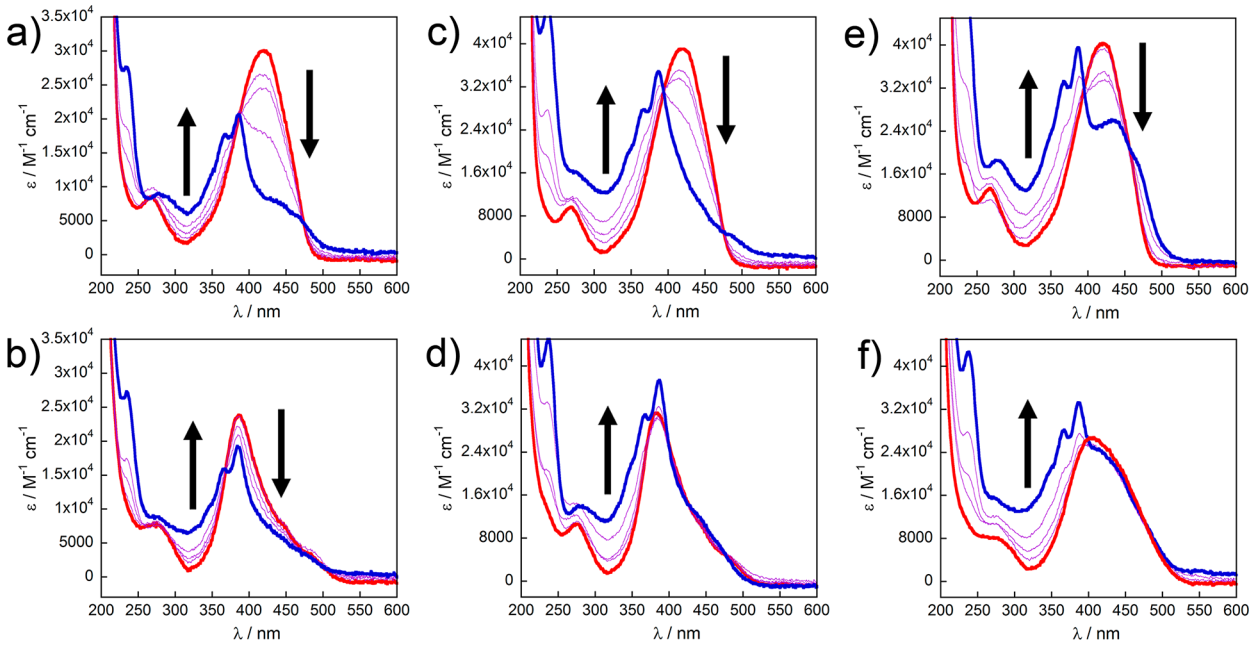

Figure 4. Steady-state UV−vis spectra of donor−acceptor (**DA**, blue lines), control peptides (**C**, red lines), and mixtures (10:90, 25:75, and 50:50 **DA**:**C**, purple lines): (a) **DA-6** and **C-6**, unassembled (pH 8); (b) **DA-6** and **C-6**, assembled (pH 4); (c) **DA-3** and **C-3**, unassembled (pH 8); (d) **DA-3** and **C-3**, assembled (pH 4); (e) **DA-2** and **C-2**, unassembled (pH 8); and (f) **DA-2** and **C-2**, assembled (pH 4) at a concentration of 2.2 μM. Arrows indicate the spectral trend with increasing concentration of **DA** peptide.

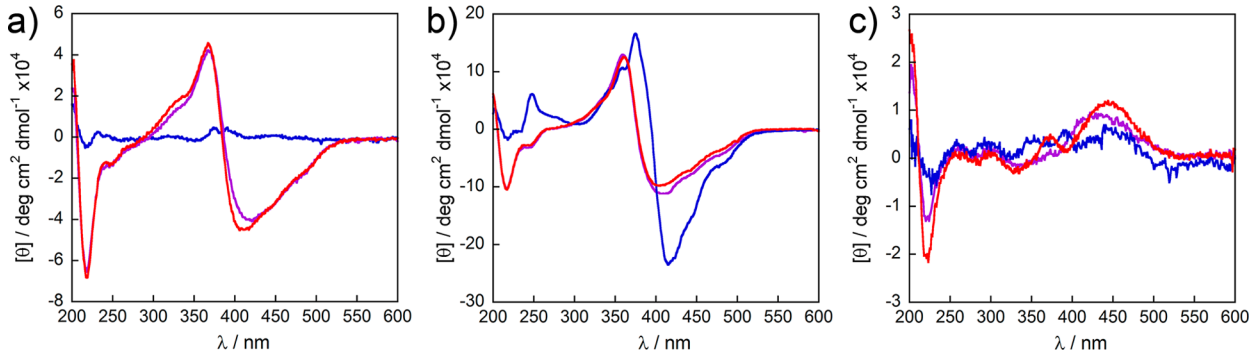

Figure 5. Circular dichroism spectra of donor−acceptor (blue lines), control peptides (red lines), and mixtures (10:90 **DA**:**C**, purple lines) under assembled conditions (pH 4) at a concentration of 44 μM: (a) **DA-6** and **C-6**, (b) **DA-3** and **C-3**, and (c) **DA-2** and **C-2**.

intertwining of two or more structures. The nanostructures formed by **DA-6** (Figure 3a) are substantially thicker (ca. 10−12 nm) suggesting that the positioning of the NDI moiety on the external amino acid side chain causes the peptide to exhibit a higher degree of hydrophobicity at its termini in comparison to the other peptides that alters the hierarchical process. Furthermore, the donor−acceptor peptide structures appear to generally have lower aspect ratios in comparison to those of the acylated controls. The structures formed from a mixture of **DA-2** and **C-2** (Figure 3f) appear to be unique with less structure intertwining, slightly thicker diameters (8−10 nm), and relatively longer aspect ratios. Importantly, all NDI-containing samples revealed the preference for 1-D assembly despite the added perturbation of the large aromatic diimide core.

Electronic Absorption. The acid-triggered self-assembly of the peptides also induces exciton coupling between the transition dipoles of the embedded OT4 chromophores leading to perturbations in the steady-state absorption spectra, as we and others have previously demonstrated with peptidic triblock architectures.[36−38,41−44] Therefore, these data were acquired for each donor−acceptor peptide (blue lines), acylated control peptide (red lines), and various **DA**:**C** mixtures (10:90, 25:75, and 50:50, purple lines) in both basic and acidic aqueous environments (Figure 4). In general, each acylated control peptide displays a blue shift in the absorption λ_{max} of the OT4 chromophore upon acidic-triggered assembly, which is indicative of cofacial H-like aggregation.[45] Interestingly, while control peptides **C-6** and **C-3** display larger blue shifts (32−34 nm), **C-2** shifts only 13 nm and exhibits a more pronounced low-energy shoulder, reflecting the influence of the bulky acylated lysine residues in close proximity to the OT4 chromophore. The spectra of the 100% **DA** peptides (Figure 4, blue lines) show minimal perturbation of the NDI absorbance between basic and acidic environments and are similar for each peptide. This suggests these units remain electronically isolated even in the aggregate nanomaterial states. Although the vibronic coupling associated with the NDI chromophore did not vary significantly with position on the peptide, the spectral signatures associated with the OT4 absorptions in these molecules were quite different in the basic

DOI: 10.1021/jacs.5b12001
J. Am. Chem. Soc. 2016, 138, 3362−3370

pH molecular state. For **DA-6**, the defined OT4 absorption present at basic pH in the region greater than 425 nm is less pronounced upon acidification and assembly, whereas this feature persists quite noticeably in **DA-2**. In contrast, **DA-3** shows very little variation between the basic and acidic pH extremes, which we interpret as pre-existing extents of self-association at the basic pH.

The **DA-C** mixtures, under both molecular (basic pH) and assembled (acidic pH) conditions showed absorption features that appeared to have additive contributions from the two different components, indicating that the electronic interactions in the co-assemblies are not substantially different than those within the neat **DA** nanostructures. It should be noted that the extinction coefficient for the OT signature is reduced in the **DA** peptides, so a constant OT4 absorption feature is not present in the unassembled mixtures of **DA-x** and **C-x**.

Circular Dichroism. CD spectra for **DA** and **C** peptide in acidic (pH 4) aqueous environments are shown in Figure 5. At basic pH, where the molecules remain isolated and dissolved, the control peptides display no meaningful absorption within the wavelength range of the OT4 chromophore $\pi-\pi^*$ transition. Upon acidification and assembly, Cotton effects are evident (red lines) that suggest chromophore interaction within the chiral environment created by the assembled peptide scaffolds. Control peptides **C-6** and **C-3** show similar behavior, each inducing a negative bisignate signal, although that for **C-3** is over twice as intense. As was previously seen in the absorption studies, **C-2** also exhibits much different behavior in its CD spectrum, suggesting a unique supramolecular assembly in comparison to the other acylated control peptides. Again, this could possibly be due to the relatively bulky lysine residue situated in close proximity to the embedded quaterthiophene chromophore. The **DA** peptide assemblies also revealed major differences. While **DA-6** and **DA-2** show no meaningful signals corresponding to the OT4 chromophores in an acidic environment, weak signals consistent with the NDI subunit are evident in **DA-6**. In contrast, **C-3** exhibits a strong negative bisignate Cotton effect in the absorption range of the OT4 and NDI moieties while assembled in acidic solution. **C-2** shows essentially no meaningful signal in the chromophore absorbance range in acidic solution.

CD spectra of donor–acceptor/control mixtures in acidic solution (10:90 DA:C, purple lines) were also obtained and compared to those of the pure components. In the case of **DA-6**/**C-6** and **DA-2**/**C-2** pairs, addition of **DA** correlates with decreasing molar ellipticity. Alternatively, the mixing of pair **DA-3**/**C-3** causes a slight increase in signal intensity, due to the fact that the molar ellipticity of pure, assembled **C-3** is significantly larger than that of **DA-3**. These spectral studies demonstrate that, while the structures of each family of peptides are quite similar and all have been shown to form 1-D nanostructures by TEM, the position of the lysine residues elicits differences in intermolecular electronic coupling at the supramolecular level.

3. Photophysical Characterization of Charge Transfer.

Steady-State Photoluminescence. Steady-state photoluminescence signatures are also perturbed upon interaction of emissive chromophores through self-assembly. Following excitation of the OT4 chromophore, the acylated control peptides (**C-6**, **C-3**, **C-2**) display nearly identical emission in basic environments and dramatic quenching and red-shifting upon assembly (Figure 6), indicative of excimer formation (red lines). Radiative emission does not occur in unassembled or assembled

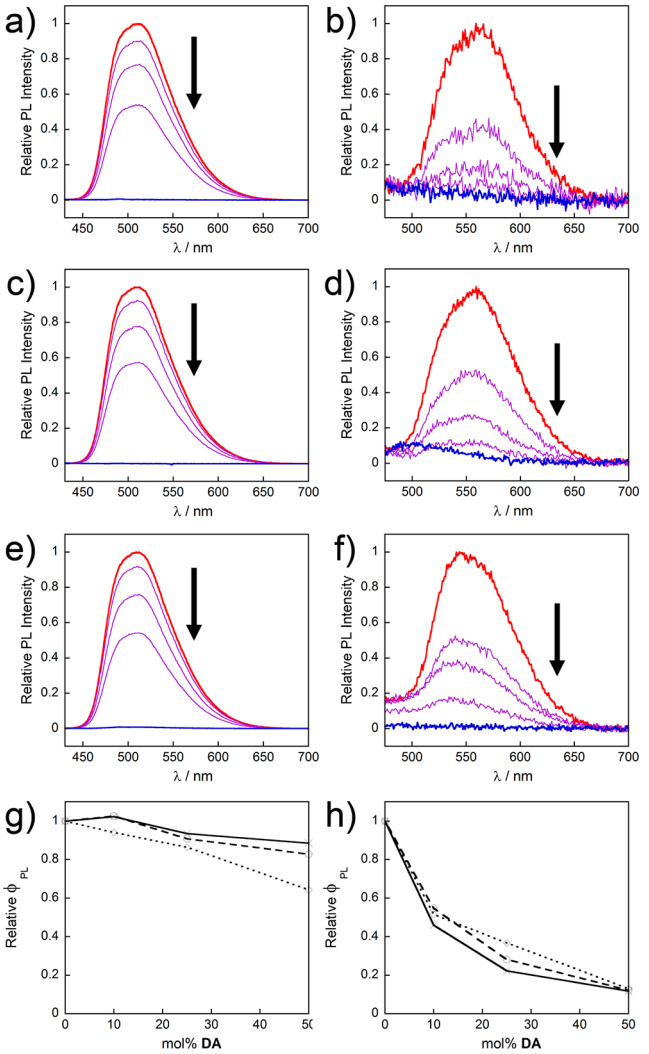

Figure 6. Steady-state emission spectra of donor–acceptor (**DA**, blue lines), control peptides (**C**, red lines), and mixtures (10:90, 25:75, and 50:50 **DA**:**C**, purple lines): (a) **DA-6** and **C-6**, unassembled (pH 8); (b) **DA-6** and **C-6**, assembled (pH 4); (c) **DA-3** and **C-3**, unassembled (pH 8); (d) **DA-3** and **C-3**, assembled (pH 4); (e) **DA-2** and **C-2**, unassembled (pH 8); and (f) **DA-2** and **C-2**, assembled (pH 4). Plots of relative (to 100% **C**) quantum yield vs mol % **DA** for each donor–acceptor and control pair (**DA-6** and **C-6**, solid lines; **DA-3** and **C-3**, dashed lines; **DA-2** and **C-2**, dotted lines) while (g) unassembled and (h) assembled. Arrows indicate the spectral trend with increasing concentration of DA peptide.

samples of the donor–acceptor peptides (**DA-6**, **DA-3**, **DA-2**, blue lines), as can be expected due to electron transfer. Therefore, increasing ratios of **DA**:**C** causes enhanced photoluminescence quenching (purple lines). Interestingly, more dramatic quenching of the photoluminescence occurs at the same mole percent of donor–acceptor peptide within assembled samples, as shown in the relative photoluminescence quantum yield vs mol% **DA** plots (Figures 6g,h). While minimal change occurs for the unassembled mixtures of 10% **DA**:90% **C** relative to the 100% **C**, assembled 10:90 mixtures retain only ca. 50% relative quantum yield. Unassembled samples containing 50% **DA** are quenched to 87%–64% relative quantum yield, while assembled samples are much more dramatically reduced to 13%–11%. These results not only suggest that electron transfer occurs in assemblies, but also that

DOI: 10.1021/jacs.5b12001
J. Am. Chem. Soc. 2016, 138, 3362–3370

a greater fraction of excited donors are quenched by electron transfer when assembled. This likely reflects that excitons delocalize within the assembled arrays prior to electron transfer to the NDI acceptor units, a process that cannot occur within the unassembled mixtures.

Dynamics of Charge Separation in Dyads and Dyad Assemblies. As described above, the electron donor (OT4) and acceptor (NDI) moieties incorporated into the dyad structures were chosen specifically such that their relative HOMO and LUMO energies enable electron transfer from OT4 to NDI but *not* from NDI to OT4; furthermore, their HOMO−LUMO gaps inhibit energy transfer from photoexcited OT4 to NDI. Based on this design principle, any charge transfer that follows photoexcitation of OT4 moieties should only produce NDI^- and $OT4^+$ radicals, which both have distinct spectroscopic signatures.[46,47] As formation of persistent charges could not be identified from steady-state UV−vis measurements, broadband ultrafast transient absorption spectroscopy was used to probe the formation of charged species and assess how the properties of the dyad structures control charge separation and recombination kinetics when they are assembled and unassembled.

For these measurements the OT4 moiety was photoexcited at 400 nm, with resulting evolution in transient absorptivity probed between 450 and 1150 nm with an experimental time resolution of 90 fs. This excitation wavelength was chosen for convenience, but approaches the absorption onset for NDI. Control measurements were also made at 480 nm, at the red side of the steady-state OT4 spectrum (Figure S26b). The similarity in the spectral dynamics observed at the two excitation wavelengths supports that the OT4 moiety is selectively excited at 400 nm. Variations in spectral dynamics with excitation fluence were also examined to ensure that spectral dynamics were not the effect of two-photon excitation or dynamics of biexcitations (Figure S27), as described below.

Figure 7a presents the spectral dynamics of unassembled **DA-2** dyads in aqueous solution following excitation at 400 nm. Five transient spectral features can be identified from this spectral progression: a negative signal below 475 nm, which corresponds with bleach of the OT4 ground-state absorption band; three transient absorption bands at ∼500, 670, and 1100 nm; and a broad absorption band centered around 775 nm. All features appear almost immediately upon excitation, whereas the broad band around 775 nm disappears within a few hundred femtoseconds, and the others disappear on a time scale of picoseconds.

Figure 8a,b presents principal spectral and kinetic components obtained from a global analysis of the data presented in Figure 7a (analysis details in SI); these indicate that the spectral dynamics observed following excitation is associated with two spectral patterns and two photoinduced responses. Figure 8a reveals that the band centered near 775 nm that decays within the first picosecond after excitation resembles the spectrum of isolated OT4 photoexcited to its S_1 state as measured in previous works.[48−50] In contrast, the remaining features closely match signatures of reduced or oxidized components of the dyad: the bands at 500 and 1100 nm (and a shoulder at 750 nm) match features in the spectra of reduced NDI,[46,51] whereas the band at 670 nm matches the well-known absorption band of oxidized OT4.[47] The presence of these bands and their simultaneous decay with concomitant recovery of the OT4 bleach indicate that photoexcitation induces charge separation between the donor and acceptor moieties within the

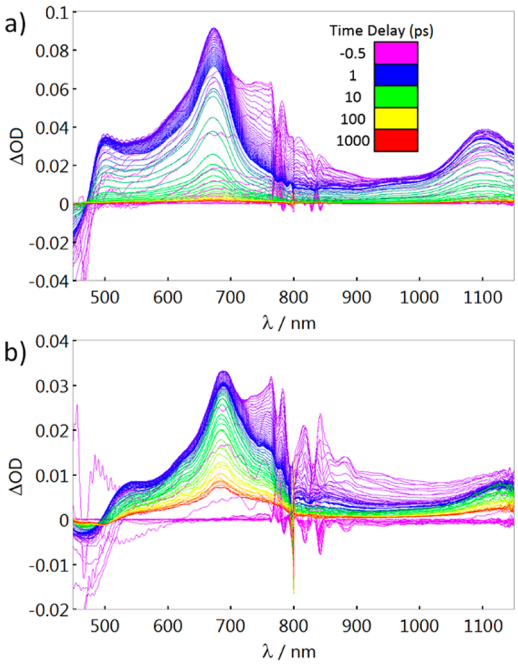

Figure 7. Spectral dynamics following photoexcitation of (a) unassembled and (b) assembled **DA-2** at 400 nm. Spectra were collected in 50 fs increments from −0.5 to 1 ps, followed by logarithmically dispersed delays between 1 and 1000 ps.

unassembled dyad; this photoinduced separation is followed by charge recombination on a time scale of several picoseconds.

There are no spectral or temporal signatures suggesting that peptide regions serve as charge acceptors or donors at any stage following excitation. However, principal kinetic components plotted in Figure 8b demonstrate that charge separation occurs from the photo prepared excited state via two modes: (1) promptly (within the time resolution of the experiment) and (2) delayed, on a timescale of ∼300 fs from the S_1 state of the OT4 moiety. The observation of two modes of charge separation suggests that conformation or charge of the bridging peptide impacts the electronic coupling between the OT4 and NDI moieties. The transients in Figure 8b also reveal that charge separated species recombine predominantly on a ∼5 ps time scale, with a small fraction persisting into the hundreds of picoseconds to nanoseconds regime. Observation of two recombination time scales may reflect differences in the reorganization energy for charge recombination due to peptide conformation or charge, but may also arise from the presence of some assembled dyads in solution.[52] Characteristic decay time scales of the local OT4 excitation and charge-separated pairs were obtained by fitting the temporal components obtained through global analysis to single or biexponential decay functions convoluted with the instrument response. Values of fitting parameters are presented in Table 1.

Figure 7b presents the transient spectral dynamics observed following 400 nm excitation of a suspension of assembled **DA-2** dyads in aqueous solution. The shapes and positions of the transient spectra are qualitatively similar to those observed with unassembled dyads, except that the 500, 670, and 1100 nm transient bands associated with charge-separated species are red-shifted by 20−25 nm and also exhibit somewhat broader line shapes. Furthermore, the short-lived S_1 absorption of OT4 extends over 1100 nm and overlaps the absorption of NDI^- in the near-IR. This breadth and substantial redshift in the OT4

DOI: 10.1021/jacs.5b12001
J. Am. Chem. Soc. 2016, 138, 3362−3370

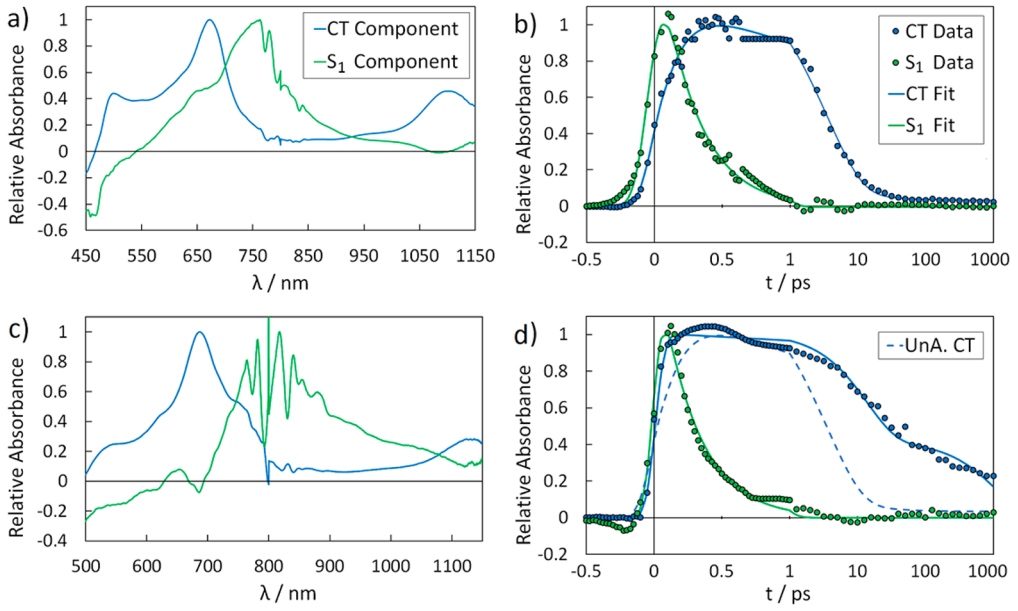

Figure 8. Principal spectral (a,c) and kinetic (b,d) components from the global analysis of time-dependent spectra from 400 nm excitation of **DA-2** presented in Figure 7a (unassembled: a, b) and Figure 7b (assembled: c, d). Here, the blue traces correspond with charge-separated species, and the green traces correspond with the OT4 excited singlet. The kinetic progression of the assembled samples (d) is similar to that observed for unassembled aggregates (b) for the S_1 components, but 1−2 orders of magnitude longer for the charge-separated state.

Table 1. Parameters for Exponential Fits to Kinetic Traces Obtained from a Global Analysis of Transient Spectra of Photoexcited DA-2 Dyads[a]

parameter	unassembled	95% CI	assembled	95% CI
f_{CS1}	0.958	0.893 to 1.057	0.585	0.461 to 0.709
τ_{CS1} (ps)	4.84	3.35 to 6.35	13.7	6.4 to 26.2
f_{CS2}	0.042	−0.012 to 0.097	0.415	0.286 to 0.544
τ_{CS2} (ps)	constant	–	1106	461 to constant
τ_{S1}	0.269	0.203 to 0.305	0.276	0.228 to 0.330

[a]95% confidence intervals (CI) were predicted using a nonlinear least-squares fitting error analysis. A single exponential decay was fit to the OT4 S_1 decay, whereas the decay of charge-separated states (CS) was fit with a biexponential decay. For the latter, f_{CSn} is the fraction of CS pairs with lifetime τ_{CSn}.

absorption are consistent with stacked chromophores in assemblies.

Figure 8c,d presents the corresponding principal spectral and kinetic components obtained through global analysis. Spectral components plotted in Figure 8c are highly similar to those obtained with unassembled dyads. Furthermore, the signature of S_1 OT4 decays on comparable time scales for both cases (270 fs, Table 1), suggesting that charge-transfer dynamics are similar in the two environments and that any energy transfer along the OT4 core of an assembly may be limited by the rate of ultrafast charge separation. In contrast, the kinetics of charge recombination differs markedly: whereas recombination occurs on picosecond time scales in unassembled dyads, roughly 40% of separated charges persist for time scales of hundreds of picoseconds to nanoseconds in assemblies. This observation indicates that stacking of the OT4 moieties (and potentially also NDI moieties) provides the ability for charge pairs to migrate or separate along the assemblies. Alternatively, assembly of the dyads may change the driving force or reorganization energy for charge recombination of proximal charge pairs. Nonetheless, the data demonstrate that an increase in the charge-separation lifetime is achieved through aggregation.

Only modest differences in the transient spectral dynamics are observed for both unassembled and assembled dyads upon increasing the excitation wavelength from 400 to 480 nm and with no appreciable change in excited-state and charge-pair lifetimes (Figure S26). Little fluence dependence is observed in the spectral dynamics measured with the unassembled or assembled dyads as well, confirming that charge separation observed here is not due to two-photon transitions or exciton annihilation. In contrast, the transient spectra of control assemblies exhibit signatures of $OT4^+$ at high fluence and long-lived OT4 S_1 signal at lower fluences (Figure S28). This demonstrates that donor−acceptor charge separation is highly competitive with multi-photon excitation and annihilation mechanisms along the OT4 core.

We collected transient absorption data for all dyad structures reported in this Article and find that the transient spectroscopy of **DA-2** is representative of all structures. Transient absorption data associated with **DA-3** and **DA-6** (unassembled and assembled) are presented in Figure S30, as are comparisons of the time-dependent behaviors of features associated with $OT4^+$, NDI^-, and OT4* from all dyad structures (Figure S31). In general, spectral dynamics and time dependence across the set of unassembled or assembled dyads are similar, regardless of the length of the bridging peptide and therefore the donor−acceptor separation. Hence, we conclude that the dynamics of photoinduced electron transfer and recombination is not impeded by D−A distance on the length scales of the peptide linkers studied here, and our general conclusions about charge-transfer in isolated and assembled dyads are valid for all three structures.

Figure 9 presents absorption transients collected at 1100 nm under identical excitation fluences for control (**C-2**), dyad (**DA-2**), and mixed (**C-2**/**DA-2**) assemblies. Significantly different time-dependent behavior is observed at this probe wavelength for control and dyad assemblies (green and blue symbols and fit

DOI: 10.1021/jacs.5b12001
J. Am. Chem. Soc. 2016, 138, 3362−3370

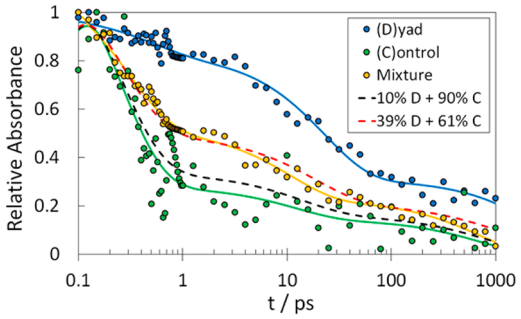

Figure 9. Relative time-dependent spectral intensity (1100−1150 nm) of the NIR absorption of NDI^{-} and excited OT4 for assemblies of **DA-2**, **C-2**, and a 10:90 mixture. Mixture data are compared to the anticipated 10:90 and fitted 39:61 combinations of dyad and control traces, revealing a disproportionate dependence on dyad concentration—a manifestation of energy migration through the assembly.

lines, respectively). Transient absorption from an assembly of a 10%−90% **DA:C** mixture exhibits intermediate behavior (yellow symbols and fit line). The intensity decay at this wavelength for mixed assemblies cannot be recovered through a proportionate combination of the control and dyad traces (black dashed line, 10%−90%), but rather by a 39%−61% combination of these pure-assembly transients (red dashed line). This comparison indicates that photoexcitation enables some degree of delocalization or energy transfer and supports observations from steady-state measurements (e.g., Figure 5h). On statistical grounds, this suggests an effective delocalization over three or four donors.[53,54]

CONCLUSION

In conclusion, we have synthesized a library of novel donor−acceptor π-peptide hybrids, which can self-assemble to form 1-D nanostructures in aqueous media. These peptides undergo photoinduced electron transfer from the embedded OT4 donor moiety to the peripherally attached NDI acceptor units after excitation of the donor, as demonstrated explicitly with transient absorption spectroscopy. Electron transfer is observed to occur both promptly (<100 fs) and with a delay of 270 fs for assembled and unassembled dyads, suggesting that structural heterogeneities (e.g., conformation or peptide charge) likely impact charge-separation dynamics. Furthermore, assembly of donor−acceptor hybrids results in a 10−100-fold increase in the charge-separation lifetime, with charges persisting into the nanosecond time regime. Through co-assembly we diluted the key donor−acceptor unit within a matrix of energy-harvesting donor peptides, thus offering the prospect for directed energy migration through this nanostructured matrix to the acceptor dopant site. Indeed, observations of both enhancements in the steady-state quenching of donor photoluminescence and transient spectral responses that are disproportionate with respect to dyad and donor-only composition indicate that such a process is operative. In general, this supramolecular platform offers the unique possibility of merging electric-field creation into biologically relevant nanomaterials, and our future investigations will seek to understand how such fields can alter or impact cellular physiology.

ASSOCIATED CONTENT

Supporting Information

The Supporting Information is available free of charge on the ACS Publications website at DOI: 10.1021/jacs.5b12001.

General experimental conditions and procedures, NMR and ESI spectra, HPLC traces, TEM images for control peptides, additional ultrafast spectra, and spectral analysis procedures (PDF)

AUTHOR INFORMATION

Corresponding Author

*tovar@jhu.edu

Notes

The authors declare no competing financial interest.

[⊥]Taken in part from the Ph.D. thesis of A.M.S. (Johns Hopkins University, 2015). Current position: Postdoctoral Fellow (Cancer Research Training Award), National Cancer Institute, Frederick, MD 21702.

ACKNOWLEDGMENTS

We thank Johns Hopkins University, the U.S. Department of Energy, Office of Basic Energy Sciences (DE-SC0004857 to J.D.T. for synthesis of peptide nanomaterials), and the National Science Foundation (DMR-1407493 to J.D.T. for electric field creation in biomaterials) for generous support. A.M.S. was the recipient of a Harry and Cleio Greer Fellowship.

REFERENCES

(1) Forciniti, L.; Guimard, N. K.; Lee, S.; Schmidt, C. E. *J. Mater. Chem.* **2010**, *20* (40), 8865.
(2) Wang, Y.; Corbitt, T. S.; Jett, S. D.; Tang, Y.; Schanze, K. S.; Chi, E. Y.; Whitten, D. G. *Langmuir* **2012**, *28* (1), 65−70.
(3) Traina, C. A.; Bakus, R. C., II; Bazan, G. C. *J. Am. Chem. Soc.* **2011**, *133* (32), 12600−12607.
(4) Wong, J. Y.; Langer, R.; Ingber, D. E. *Proc. Natl. Acad. Sci. U. S. A.* **1994**, *91* (8), 3201−3204.
(5) Zhao, H.; Zhu, B.; Sekine, J.; Luo, S.-C.; Yu, H. *ACS Appl. Mater. Interfaces* **2012**, *4* (2), 680−686.
(6) Abidian, M. R.; Corey, J. M.; Kipke, D. R.; Martin, D. C. *Small* **2010**, *6* (3), 421−429.
(7) Mawad, D.; Stewart, E.; Officer, D. L.; Romeo, T.; Wagner, P.; Wagner, K.; Wallace, G. G. *Adv. Funct. Mater.* **2012**, *22* (13), 2692−2699.
(8) Gumus, A.; Califano, J. P.; Wan, A. M. D.; Huynh, J.; Reinhart-King, C. A.; Malliaras, G. G. *Soft Matter* **2010**, *6* (20), 5138.
(9) Guarino, V.; Alvarez-Perez, M. A.; Borriello, A.; Napolitano, T.; Ambrosio, L. *Adv. Healthcare Mater.* **2013**, *2* (1), 218−227.
(10) Schmidt, C. E.; Shastri, V. R.; Vacanti, J. P.; Langer, R. *Proc. Natl. Acad. Sci. U. S. A.* **1997**, *94* (17), 8948−8953.
(11) Brea, R. J.; Castedo, L.; Granja, J. R.; Herranz, M. A.; Sanchez, L.; Martin, N.; Seitz, W.; Guldi, D. M. *Proc. Natl. Acad. Sci. U. S. A.* **2007**, *104* (13), 5291−5294.
(12) Kim, S. H.; Parquette, J. R. *Chem. Lett.* **2014**, *43* (10), 1634−1636.
(13) Wasielewski, M. R. *Chem. Rev.* **1992**, *92* (3), 435−461.
(14) Imahori, H.; Guldi, D. M.; Tamaki, K.; Yoshida, Y.; Luo, C.; Sakata, Y.; Fukuzumi, S. *J. Am. Chem. Soc.* **2001**, *123* (27), 6617−6628.
(15) Imahori, H.; Tamaki, K.; Guldi, D. M.; Luo, C.; Fujitsuka, M.; Ito, O.; Sakata, Y.; Fukuzumi, S. *J. Am. Chem. Soc.* **2001**, *123* (11), 2607−2617.
(16) Liddell, P. A.; Sumida, J. P.; Macpherson, A. N.; Noss, L.; Seely, G. R.; Clark, K. N.; Moore, A. L.; Moore, T. A.; Gust, D. *Photochem. Photobiol.* **1994**, *60* (6), 537−541.
(17) Kuciauskas, D.; Lin, S.; Seely, G. R.; Moore, A. L.; Moore, T. A.; Gust, D.; Drovetskaya, T.; Reed, C. A.; Boyd, P. D. W. *J. Phys. Chem.* **1996**, *100* (39), 15926−15932.
(18) Liddell, P. A.; Kuciauskas, D.; Sumida, J. P.; Nash, B.; Nguyen, D.; Moore, A. L.; Moore, T. A.; Gust, D. *J. Am. Chem. Soc.* **1997**, *119* (6), 1400−1405.

DOI: 10.1021/jacs.5b12001
J. Am. Chem. Soc. 2016, 138, 3362−3370

(19) Kuciauskas, D.; Liddell, P. A.; Lin, S.; Johnson, T. E.; Weghorn, S. J.; Lindsey, J. S.; Moore, A. L.; Moore, T. A.; Gust, D. *J. Am. Chem. Soc.* **1999**, *121* (37), 8604−8614.
(20) Liddell, P. A.; Kodis, G.; Moore, A. L.; Moore, T. A.; Gust, D. *J. Am. Chem. Soc.* **2002**, *124* (26), 7668−7669.
(21) Beckers, E. H. A.; Meskers, S. C. J.; Schenning, A. P. H. J.; Chen, Z.; Würthner, F.; Marsal, P.; Beljonne, D.; Cornil, J.; Janssen, R. A. J. *J. Am. Chem. Soc.* **2006**, *128* (2), 649−657.
(22) Wasielewski, M. R. *Acc. Chem. Res.* **2009**, *42* (12), 1910−1921.
(23) Ahrens, M. J.; Sinks, L. E.; Rybtchinski, B.; Liu, W.; Jones, B. A.; Giaimo, J. M.; Gusev, A. V.; Goshe, A. J.; Tiede, D. M.; Wasielewski, M. R. *J. Am. Chem. Soc.* **2004**, *126* (26), 8284−8294.
(24) Rybtchinski, B.; Sinks, L. E.; Wasielewski, M. R. *J. Am. Chem. Soc.* **2004**, *126* (39), 12268−12269.
(25) Schenning, A. P. H. J.; Herrikhuyzen, J. v.; Jonkheijm, P.; Chen, Z.; Würthner, F.; Meijer, E. W. *J. Am. Chem. Soc.* **2002**, *124* (35), 10252−10253.
(26) Horne, W. S.; Ashkenasy, N.; Ghadiri, M. R. *Chem. - Eur. J.* **2005**, *11* (4), 1137−1144.
(27) Jones, G.; Vullev, V.; Braswell, E. H.; Zhu, D. *J. Am. Chem. Soc.* **2000**, *122* (2), 388−389.
(28) Fox, M. A.; Galoppini, E. *J. Am. Chem. Soc.* **1997**, *119* (23), 5277−5285.
(29) Galoppini, E.; Fox, M. A. *J. Am. Chem. Soc.* **1996**, *118* (9), 2299−2300.
(30) Polizzi, N. F.; Eibling, M. J.; Perez-Aguilar, J. M.; Rawson, J.; Lanci, C. J.; Fry, H. C.; Beratan, D. N.; Saven, J. G.; Therien, M. J. *J. Am. Chem. Soc.* **2016**, *138*, 2130.
(31) Ardoña, H. A. M.; Tovar, J. D. *Bioconjugate Chem.* **2015**, *26* (12), 2290−2302.
(32) Gao, M.; Paul, S.; Schwieters, C. D.; You, Z.-Q.; Shao, H.; Herbert, J. M.; Parquette, J. R.; Jaroniec, C. P. *J. Phys. Chem. C* **2015**, *119* (24), 13948−13956.
(33) Ardoña, H. A. M.; Tovar, J. D. *Chem. Sci.* **2015**, *6* (2), 1474−1484.
(34) Chen, L.; Revel, S.; Morris, K.; Adams, D. J. *Chem. Commun.* **2010**, *46* (24), 4267.
(35) Nalluri, S. K. M.; Ulijn, R. V. *Chem. Sci.* **2013**, *4* (9), 3699.
(36) Vadehra, G. S.; Wall, B. D.; Diegelmann, S. R.; Tovar, J. D. *Chem. Commun.* **2010**, *46* (22), 3947.
(37) Sanders, A. M.; Dawidczyk, T. J.; Katz, H. E.; Tovar, J. D. *ACS Macro Lett.* **2012**, *1* (11), 1326−1329.
(38) Sanders, A. M.; Tovar, J. D. *Supramol. Chem.* **2014**, *26* (3−4), 259−266.
(39) Bheemaraju, A.; Pourmand, M.; Yang, B.; Surampudi, S. K.; Benanti, T. L.; Achermann, M.; Barnes, M. D.; Venkataraman, D. *J. Macromol. Sci., Part A: Pure Appl.Chem.* **2011**, *48* (12), 986−993.
(40) Shao, H.; Nguyen, T.; Romano, N. C.; Modarelli, D. A.; Parquette, J. R. *J. Am. Chem. Soc.* **2009**, *131* (45), 16374−16376.
(41) Wall, B. D.; Zacca, A. E.; Sanders, A. M.; Wilson, W. L.; Ferguson, A. L.; Tovar, J. D. *Langmuir* **2014**, *30* (20), 5946−5956.
(42) Stone, D. A.; Hsu, L.; Stupp, S. I. *Soft Matter* **2009**, *5* (10), 1990.
(43) Gallaher, J. K.; Aitken, E. J.; Keyzers, R. A.; Hodgkiss, J. M. *Chem. Commun.* **2012**, *48* (64), 7961.
(44) Marty, R.; Szilluweit, R.; Sánchez-Ferrer, A.; Bolisetty, S.; Adamcik, J.; Mezzenga, R.; Spitzner, E.; Feifer, M.; Steinmann, S. N.; Corminboeuf, C.; Frauenrath, H. *ACS Nano* **2013**, *7* (10), 8498−8508.
(45) Kasha, M.; Rawls, H. R.; El-Bayoumi, M. A. *Pure Appl. Chem.* **1965**, *11* (3−4), 371−392.
(46) Bhosale, S. V.; Jani, C. H.; Langford, S. J. *Chem. Soc. Rev.* **2008**, *37* (2), 331−342.
(47) van Hal, P. A.; Beckers, E. H. A.; Meskers, S. C. J.; Janssen, R. A. J.; Jousselme, B.; Blanchard, P.; Roncali, J. *Chem. - Eur. J.* **2002**, *8* (23), 5415−5429.
(48) Zhou, J.; Yu, W.; Bragg, A. E. *J. Phys. Chem. Lett.* **2015**, *6* (17), 3496−3502.
(49) Lap, D. V.; Grebner, D.; Rentsch, S. *J. Phys. Chem. A* **1997**, *101* (2), 107−112.
(50) Benincori, T.; Bongiovanni, G.; Botta, C.; Cerullo, G.; Lanzani, G.; Mura, A.; Rossi, L.; Sannicolò, F.; Tubino, R. *Phys. Rev. B: Condens. Matter Mater. Phys.* **1998**, *58* (14), 9082−9086.
(51) Ivnitski, D.; Amit, M.; Rubinov, B.; Cohen-Luria, R.; Ashkenasy, N.; Ashkenasy, G. *Chem. Commun.* **2014**, *50* (51), 6733.
(52) Jayasuriya, N.; Kagan, J.; Owens, J. E.; Kornak, E. P.; Perrine, D. M. *J. Org. Chem.* **1989**, *54* (7), 4203−4205.
(53) Herz, L. M.; Daniel, C.; Silva, C.; Hoeben, F. J. M.; Schenning, A. P. H. J.; Meijer, E. W.; Friend, R. H.; Phillips, R. T. *Phys. Rev. B: Condens. Matter Mater. Phys.* **2003**, *68* (4), 045203.
(54) Spano, F. C.; Meskers, S. C. J.; Hennebicq, E.; Beljonne, D. *J. Am. Chem. Soc.* **2007**, *129* (22), 7044−7054.

DOI: 10.1021/jacs.5b12001
J. Am. Chem. Soc. 2016, 138, 3362−3370